Effect of cyclic aging on mode I fracture energy of dissimilar metal/composite DCB adhesive joints

Moazzami, M.; Ayatollahi, M. R.; Akhavan-Safar, A.; Teixeira De Freitas, S.; Poulis, J. A.; da Silva, L. F.M.

DOI
10.1016/j.engfracmech.2022.108675

Publication date
2022

Document Version
Final published version

Published in
Engineering Fracture Mechanics

Citation (APA)
Moazzami, M., Ayatollahi, M. R., Akhavan-Safar, A., Teixeira De Freitas, S., Poulis, J. A., & da Silva, L. F. M. (2022). Effect of cyclic aging on mode I fracture energy of dissimilar metal/composite DCB adhesive joints. *Engineering Fracture Mechanics*, *271*, Article 108675. https://doi.org/10.1016/j.engfracmech.2022.108675

Engineering Fracture Mechanics 271 (2022) 108675

Contents lists available at ScienceDirect

Engineering Fracture Mechanics

journal homepage: www.elsevier.com/locate/engfracmech

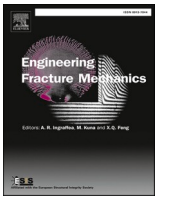

Effect of cyclic aging on mode I fracture energy of dissimilar metal/composite DCB adhesive joints

M. Moazzami [a], M.R. Ayatollahi [a], A. Akhavan-Safar [b,*], S. Teixeira De Freitas [c], J.A. Poulis [c], L.F.M. da Silva [d]

[a] Fatigue and Fracture Research Laboratory, Center of Excellence in Experimental Solid Mechanics and Dynamics, School of Mechanical Engineering, Iran University of Science and Technology, Tehran, Iran
[b] Institute of Science and Innovation in Mechanical and Industrial Engineering (INEGI), Porto, Portugal
[c] Structural Integrity Group, Faculty of Aerospace Engineering, Delft University of Technology, GB Delft, the Netherlands
[d] Department of Mechanical Engineering, Faculty of Engineering, University of Porto, Portugal

ARTICLE INFO

Keywords:
Mode I fracture energy
FTIR
Dissimilar DCB
Cyclic aging
Moisture diffusion

ABSTRACT

In some industrial applications, adhesive joints are cyclically exposed to a moist environment, where cyclic moisture absorption and desorption can significantly alter the fracture energy of the bonded joints. Most previous studies are based on monotonic aging conditions, while the performance of bonded joints under cyclic aging is not well explored The aim of the current study is to investigate the effect of cyclic aging on mode I fracture energy of dissimilar DCB (double cantilever beam) adhesive joints. Accordingly, bulk adhesive plates were manufactured and exposed to 4 aging cycles. After the aging process, at different exposure times, the aged adhesive plates were used to bond dissimilar Al/GFRP substrates using a secondary adhesive. Then the prepared DCBs were tested and subsequently the mode I fracture energy of the adhesive was determined. Meanwhile, using gravimetrical tests and numerical simulation, moisture diffusion of the adhesive layer in different exposure times was analysed. Using experimental and numerical results, the variation of fracture energy as a function of moisture uptake was studied. In addition, glass transition temperature (T_g) and chemical bonding of the aged adhesive were analysed in different aging cycles. The results showed that by increasing the number of aging cycles, the reduction rate of mode I fracture energy between the aging cycles decreases.

1. Introduction

The adhesive joining technology is extensively used in different industries due to its advantages in comparison with traditional joints such as a more uniform stress distribution and the possibility of bonding dissimilar materials such as composites, polymers, and metals [1]. The adhesive joining technique is a suitable technology for bonding fiber reinforced polymer substrates [2]. Glass fiber reinforced polymer (GFRP) composites have received attention in recent years due to their reasonable cost and their outstanding mechanical properties [3,4]. Simultaneous application of GFRP components and metal structures generated a growing research interest in making adhesive joints between dissimilar materials [5–8].

One of the basic parameters used in damage analysis of these types of bonded joints is fracture energy. For mode I fracture energy

* Corresponding author.
E-mail address: Aakhavan-Safar@inegi.up.pt (A. Akhavan-Safar).

https://doi.org/10.1016/j.engfracmech.2022.108675
Received 12 March 2022; Received in revised form 16 July 2022; Accepted 20 July 2022
Available online 22 July 2022

analysis, standards suggest DCB specimens with the same substrates [9]. However, some researchers shared that joint configuration can affect fracture energy [10]. Based on these results, for a precise measurement of mode I fracture energy in dissimilar joints, performing a DCB fracture test using different substrates to come as close as possible to the real practice is recommended [11]. In DCB adhesive joints with different substrates, obtaining mode I loading is a challenge. Previous researchers developed different techniques for mode I fracture tests in dissimilar DCB specimens [12,13]. Some researchers used the criterion based on the equivalent flexural stiffness of the two substrates to obtain pure mode I loading [13]. Wang et al. [12] proposed a new criterion based on the equivalent longitudinal strain distribution at the interface of the substrates. They observed that the new criterion decreases the mode-mixity (mode II/mode I) in dissimilar DCB joints in comparison with the equivalent flexural stiffness criterion.

In many industrial applications such as marine structures [3,14], adhesive materials are exposed to high humidity environments. During the service, the moisture diffusion changes the mechanical properties of the adhesive layer and of the composite substrate. Moisture absorption reduces the tensile modulus and strength and increases the ductility of adhesives [15–17]. In addition, previous researchers revealed that moisture absorption in the adhesive layer can either increase or decrease the fracture energy of adhesive materials [18,19]. These contrary results are due to different moisture diffusion mechanisms in the adhesive layer. Fernandes et al. [18] showed that the adhesive fracture energy is a function of the aging environment. They found that saltwater diffusion improves the fracture energy while distilled water degrades fracture energy. Zheng et al. [20] studied the residual strength of CFRP/Al adhesive joints after hygrothermal aging. They concluded that the strength of the adhesive joints exhibits a non-monotonic variation during the aging process. Before 20 days, the strength decreased; whereas by 40 days, this parameter increased noticeably.

In most industrial applications, adhesive joints are exposed to cyclic moisture absorption and desorption conditions. Mubashar et al. [21] studied the failure load of single shear lap joints after different exposure times in a single cycle of moisture absorption/desorption. They observed degradation and recovery of the joint strength during the moisture absorption and desorption, respectively. Some researchers [22,23] have studied the moisture diffusion behaviour of bulk adhesive materials exposed to cyclic aging. They found that the elastic modulus and tensile strength of adhesive decrease with the number of aging cycles. A literature review showed that research on the effect of cyclic aging on the adhesive joint's properties is limited and there is a knowledge gap in cyclic aging effects.

In this paper, the effect of cyclic aging on the mode I fracture energy of DCB adhesive joint with dissimilar GFRP/aluminium substrates is studied. For this purpose, based on the results of gravimetrical tests and using Fick's law, the moisture diffusion parameters in different aging cycles were measured. Multi-layer DCBs based on the ODCB (Open DCB) concepts [18] were manufactured and tested. ODCB technique was used in order to accelerate the aging process of the adhesive layer in DCB samples. In normal DCB joints due to the geometry of the specimen, the saturation procedure takes several months. Thus, in order to accelerate the diffusion process, ODCB specimens were used, as they are able to replicate the diffusion process that occurs in an adhesive plate. Using load–displacement curves obtained from fracture tests, the mode I fracture energy for different aging conditions was determined. Using the experimentally obtained moisture diffusion parameters, the moisture distribution in the aged adhesive layer was simulated numerically after different exposure times. Finally, the variation of mode I fracture energy as a function of the moisture distribution in the adhesive layer in different aging cycles was studied for dissimilar GFRP/aluminium joints.

2. Basic theories

2.1. Fick's law equation

In order to study moisture diffusion in polymers, several models have been developed by previous investigators. The most common and simplest moisture diffusion model is Fick's law [24]. Previous authors showed that Fick's law can be used for moisture diffusion modeling in epoxy adhesives [22]. During the moisture diffusion in adhesive material, water molecules occupy the free spaces between the polymeric chains and some of them form bonding with the polar chains and turn into bound water. According to this model, the variation of the moisture concentration over the exposure time for a large plate can be calculated as follows [24]:

$$\frac{\partial C}{\partial t} = D\left(\frac{\partial^2 C}{\partial x^2}\right) \tag{1}$$

where C is moisture concentration, t is the exposure time, D is the diffusion constant, and x is the moisture diffusion direction. By Solving the Eq. (1) based on initial and boundary conditions, using the separation of variables technique, the moisture concentration distribution can be calculated. By integrating the moisture distribution equation over the thickness of the absorbent plate (h), the instantaneous moisture uptake (M_t) during the absorption process can be obtained by [24]:

$$\frac{M_t}{M_m} = \left[1 - \frac{8}{\pi^2}\sum_{n=0}^{\infty}\frac{1}{(2n+1)^2} exp\left(-\frac{(2n+1)^2\pi^2 D}{h^2}t\right)\right] \tag{2}$$

where M_m is maximum moisture content. Eq. (2) is suitable for monotonous moisture absorption for the initial dried specimen. In cyclic aging conditions, the remaining moisture from previous cycles should be considered. In the cyclic aging process, with initial moisture from previous cycles, the instantaneous moisture uptake during the absorption process can be obtained by [22]:

$$M_t = \left[1 - \frac{8}{\pi^2}\sum_{n=0}^{\infty}\frac{1}{(2n+1)^2}exp\left(-\frac{(2n+1)^2\pi^2 D}{h^2}t\right)\right] \times (M_m - M_r) + M_r \tag{3}$$

where M_r is initial moisture remained from previous cycles. For the absorption process in the first cycle M_r is equal to zero. To predict the moisture concentration during the desorption process the corresponding Fick's law gives instantaneous moisture uptake based on the following equation [25]:

$$M_t = \left[\frac{8}{\pi^2}\sum_{n=0}^{\infty}\frac{1}{(2n+1)^2}exp\left(-\frac{(2n+1)^2\pi^2 D_d}{h^2}t\right)\right] \times (M_m - M_r) + M_r \tag{4}$$

where D_d is the diffusion constant of the desorption process. In Eq. (4), M_r is minimum fractional retained moisture after drying and M_m

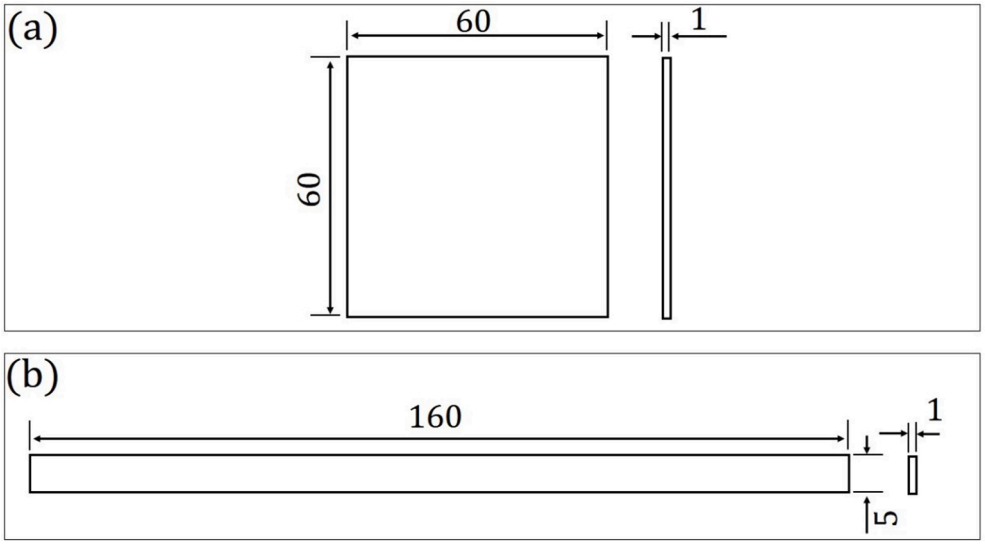

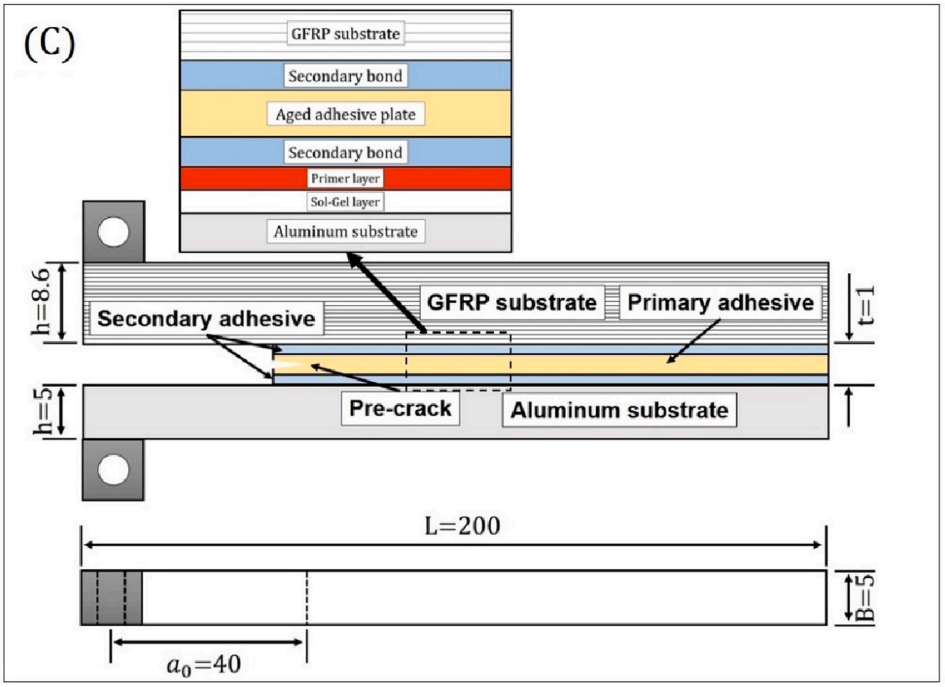

Fig. 1. Geometry of gravimetrical specimen (a), primary adhesive layer (b), and ODCB (c) (dimensions in mm and not to scale).

is maximum moisture content when the drying process starts. Previous researchers [26] showed that the diffusion constant (D) in absorption and desorption process, can be calculated from the initial slope of the moisture uptake M_t versus $\sqrt{t}$ curve where this curve is linear using the following formula.

$$D = \pi\left(\frac{h}{4M_m}\right)^2\left(\frac{M_2 - M_1}{\sqrt{t_2} - \sqrt{t_1}}\right)^2 \tag{5}$$

2.2. Data reduction approach

The most common specimen for calculation of mode I fracture energy (G_{Ic}) is the double cantilever beam (DCB), described in the American standard ASTM D3433-99 [9]. During the fracture test, the applied load (P) and the displacement of the cross-head of the testing machine (δ) are recorded at different crack lengths, a. Accordingly, the mode I fracture energy can be calculated by means of the Irwin–Kies equation [27]:

$$G_{Ic} = \frac{P_{max}^2}{2b}\frac{dC_s}{da} \tag{6}$$

where P_{max} is the maximum applied load, b is the adhesive joint width, C_s is the substrate compliance, and a is the crack length. Using the Timoshenko beam theory the relationship between specimen compliance and crack length is:

$$C_s = \frac{\delta}{P} = \frac{8a^3}{bh^3E} + \frac{12a}{5bhG} \tag{7}$$

where, E and G are the tensile and shear modulus of substrates, respectively. Based on Eqs. (6) and (7) the mode I fracture energy of DCB adhesive joints can be calculated as follows:

$$G_{Ic} = \frac{6P_{max}^2}{b^2h^3}\left(\frac{2a^2}{E} + \frac{h^2}{5G}\right) \tag{8}$$

The previous investigators showed that Eq. (8) (simple beam theory (SBT)) is suitable for fracture energy measurement of thin brittle adhesives [28].

3. Experimental procedure

3.1. Materials and manufacturing

The main adhesive chosen for this study was the two-component epoxy adhesive Araldite 2011 (Huntsman, Basel, Switzerland). For fabrication bulk specimens Araldite 2011 was mixed with a weight ratio of 100/80 (resin/hardener) using a centrifuge mixing machine, SpeedMixer DAC 150^{TM} (Hauschild, Hamm, Germany), for 2 min at 2300 rpm. After mixing, the adhesive plates were made by curing the adhesive between two thick glass plates. For controlling the thickness of the adhesive plates, 1 mm spacers made of a metal coated by a release agent were used. The adhesive plates were cured for 40 min at 80 °C according to the manufacturer's technical datasheet. These adhesive plates were cut to make square and rectangular bulk specimens. These specimens were used in both gravimetrical tests and open-DCB (ODCB) adhesive joints fabrication, respectively. ODCB specimens are a modification of the standard DCB specimens proposed by previous investigators to accelerate the moisture diffusion process [18]. ODCB specimens include three adhesive layers, instead of one (see Fig. 1c). These kinds of specimens constitute one primary adhesive and two secondary bonds. The primary adhesive is the aged rectangular specimen made of the adhesive plate, in this case, Araldite 2011. For the fabrication of ODCB specimens, the rectangular adhesive plate was exposed to the aging environment. Since the adhesive plate was not bonded to any substrate, the area exposed to the aging environment is much larger than the area of the adhesive layer in standard DCB specimens. After aging of the primary adhesive plates, they were bonded to GFRP and aluminium substrates using the epoxy adhesive Araldite 2020 (Huntsman, Basel, Switzerland). The GFRP specimens were fabricated with quadraxial E-glass fabric consisting of stacking of four unidirectional (UD) layers of E-glass lamina with the orientations of [45/90/+45/0]. This laminate was made by vacuum infusing of the fabric stacking sequence with a rubber-modified epoxy based vinyl ester resin. The GFRP laminate was cured for 1 day at 23 °C followed by 12 h at 60 °C in an oven. The mechanical properties of UD-0° E-glass lamina had been measured previously using standard specimens [12] (Table 1). On the other hand, the mechanical properties of aluminium 7075-T6 and Araldite 2011 adhesive were

Table 1
Mechanical properties of adhesive and substrates.

Material	$\mathbf{E_1}$(MPa)	$\mathbf{E_2}$(MPa)	$\mathbf{G_{12}}$(MPa)	ϑ_{12}	$\mathbf{G_{Ic}}$($\mathbf{j/m^2}$)
UD-0° E-glass lamina [12]	38,070	11,160	3951	0.28	–
Aluminium 7076-T6	71,000 ±3500	–	–	0.33	–
Araldite 2011	1550 ±150	–	–	0.45	2116

Subscript 1: longitudinal/fiber direction; Subscript 2: transverse direction.

measured in this research (Table 1). In order to measure the tensile properties of aluminum 7075-T6 and adhesive, some specimens were fabricated and tested under tensile load at ambient conditions based on ASTM E8 and ASTM D638 standards, respectively. The mode I fracture energy of adhesive was measured based on fracture tests of standard DCB specimens according to the recommendations of ASTM D5228-01 standard. For each case, three specimens were tested to show the reproducibility of the results.

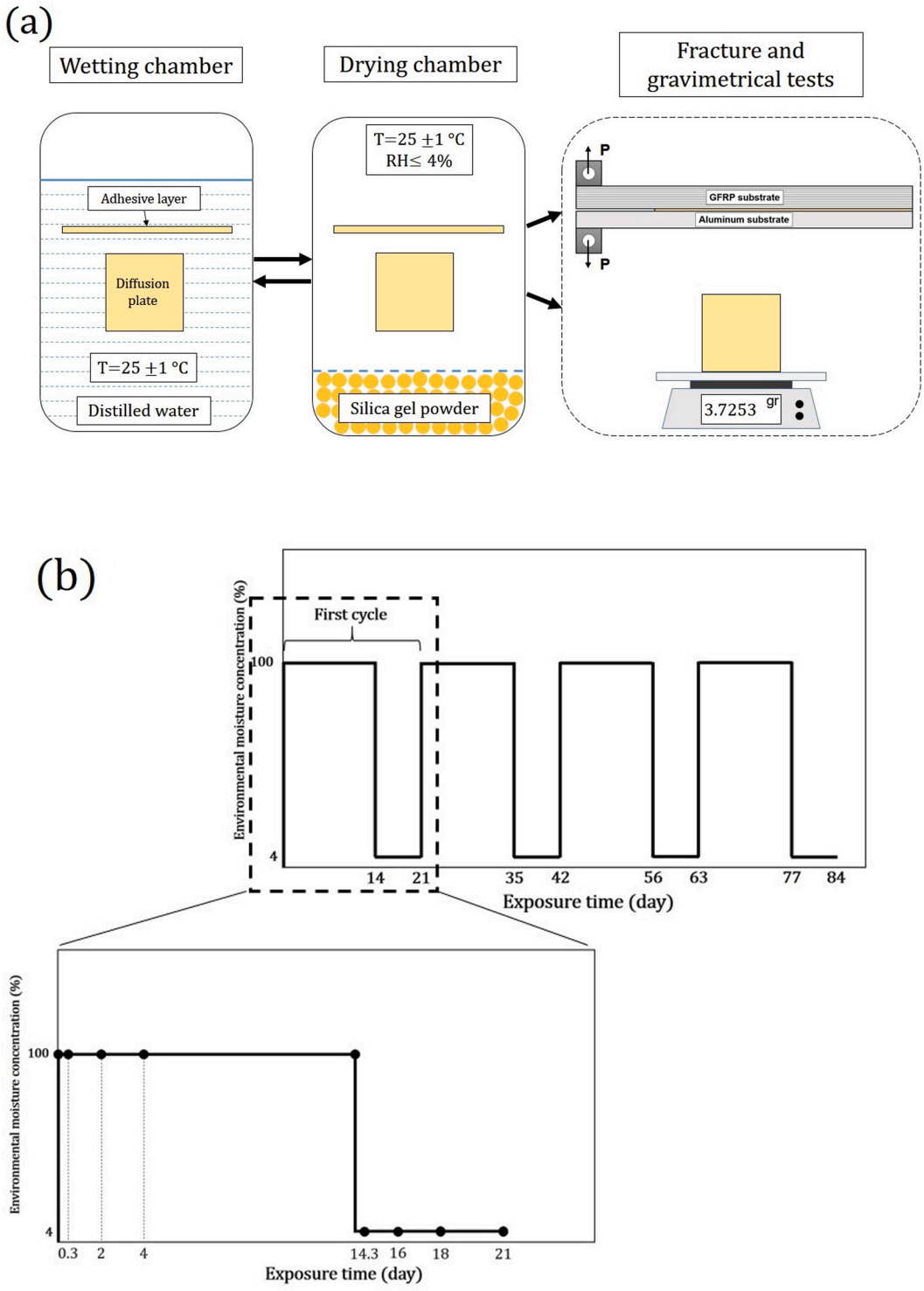

Fig. 2. Schematic representation of the aging conditions (a), aging cycles and exposure times considered for the ODCB specimens (b).

3.2. Samples' geometries

Square and rectangular bulk specimens were fabricated from the manufactured adhesive plates. The square plates were used for the measurement of moisture diffusion parameters in different aging cycles using gravimetrical tests. The rectangular adhesive specimens were used to fabricate ODCB specimens. The geometries of the employed bulk and ODCB specimens are shown in Fig. 1.

The adhesive layer dimensions are according to the mini DCB specimen geometry proposed by Costa et al [29]. They revealed that there is no significant difference in mode I fracture energy obtained using regular size DCBs [9] and mini DCBs.

The thickness of the substrates should satisfy-two conditions. The first one is avoiding plastic deformation in the aluminium substrates and failure in the GFRP laminates before adhesive layer fracture. An aluminium 7075-T6 substrate with 5 mm thickness satisfies this criterion based on numerical simulations [26]. During the numerical simulation the mode I fracture energy of the adhesive was considered as 2.116 N/mm. The second criterion which should be satisfied is the achievement of pure mode I loading condition in the adhesive layer. For this purpose, the longitudinal strain criterion was considered. Based on this criterion, it has been shown that Eq. (9) should be satisfied to get mode I loading conditions in dissimilar DCB joints [12].

$$E_{Aluminium}h^2_{Aluminium} = E_{GFRP}h^2_{GFRP} \tag{9}$$

where E and h are the flexural modulus and the substrate thickness, respectively. The flexural modulus of the GFRP had been measured previously as 21014 MPa for $[45/90/+45/0]_5/[45/90/+45/0]_5$ configuration [12]. Based on Eq. (9) the aluminium and GFRP substrates with thicknesses of 5 and 9.2 mm are satisfying the longitudinal strain criterion. Unfortunately, this criterion cannot be perfectly satisfied due to the fixed stacking sequence and thickness of the quadraxial E-glass fabric and available aluminium plate thicknesses. Due to mentioned limitations, the thickness of fabricated GFRP substrates was 8.6 mm, which is obtained with 10 layers of quadraxial E-glass fabric. The numerical simulation shows that thickness reduction of GFRP substrate to 8.6 mm increases the mode mixity ratio $\frac{G_{II}}{G_I}$ to 0.12, and this configuration can be considered as a mode I adhesive joint [12].

3.3. Aging process

The bulk specimens made of adhesive (square and rectangular specimens) were exposed to 4 aging cycles. In each cycle the absorption time was 14 days, followed by 7 days drying. The total aging duration was $(14 + 7) \times 4 = 84$ days, as shown in Fig. 2b. The temperature of the aging chamber for the wetting and drying procedures were both set to 25 ± 1 °C. The bulk specimens were

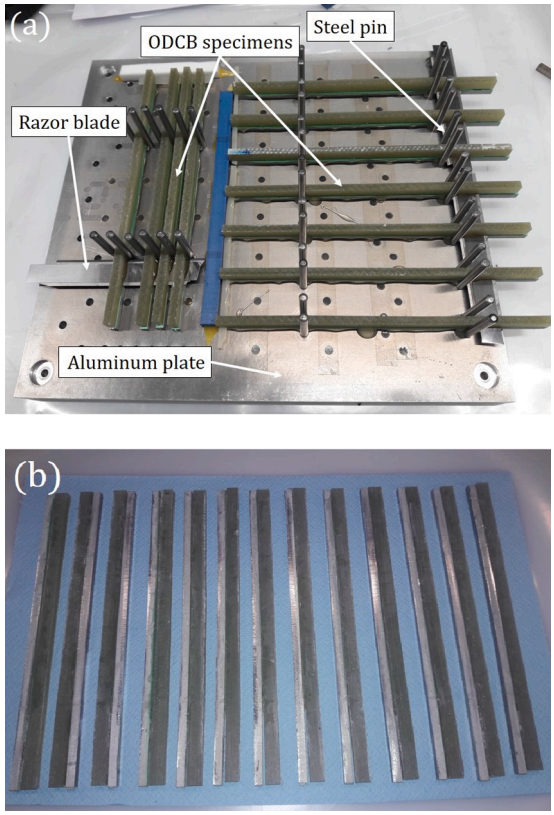

Fig. 3. ODCB specimens in aluminium mould (a) and after curing (b).

immersed in distilled water for the wetting process, while for the drying part the specimens were kept at a relative humidity of less than 4 % using a box containing silica gel powder (see Fig. 2a).

At different exposure times, selected gravimetrical specimens were taken out of the aging chamber and their moisture uptake was measured. In addition, the rectangular specimens at different aging times were bonded to substrates and were tested. Fig. 2b illustrates a schematic of exposure times in which ODCB tests were performed for one cycle. These ODCB tests were repeated at the same exposure times in the first, second and fourth cycles.

3.4. Joint manufacturing

For the fabrication of dissimilar DCB adhesive joints, the substrate surfaces were prepared for bonding. For this purpose, the bonded surfaces of the GFRP laminates were lightly sanded manually with 240 grit sandpaper without causing any damage to the glass fibres. The sanded GFRP surfaces were cleaned before and after the process using acetone. The aluminium alloy surfaces were grit blasted using aluminium oxide powder. The abrasive material was white corundum iron-free quality Corublast Super Z-EW FEPA nr.100 (Al2O3 particles with a particle size: 0.10–0.15 mm). During this process, the air pressure was set to 3 bars with the grit blasting nozzle at a distance of 4–6 cm from the specimen with an angle of 30°. The grit blasted surfaces were cleaned before and after grit blasting using a cloth soaked with acetone. Then the aluminium specimens were immersed in the sol–gel AC-130 (3 M, Unitek) bath for 90 s, and subsequently dried at room temperature for 60 min. Finally, in order to improve adhesion between the aluminium and the secondary adhesive, metal primer 3901 (3 M, Unitek) was sprayed on the grit blasted surfaces using an airbrush, and the aluminium specimens were again dried at room temperature during 60 min according to technical datasheet. After the surface treatment, aged adhesive layers made of Araldite 2011 (Fig. 1b) were abraded with sandpaper and cleaned with a cloth soaked with acetone in order to improve adhesion to the secondary adhesive. After preparation of the aged adhesive layers, they were bonded to the substrates using a secondary adhesive. For bonding the aged adhesive specimens to the substrates the Araldite 2020 was mixed with a weight ratio of 100/30 (resin/hardener) using a mixer for 1 min at 2300 rpm. After mixing, the secondary adhesive was applied on the surfaces of GFRP and aluminium substrates, using a syringe. To control the distance between the substrates, 1 mm metal spacers coated by a release agent were used on both sides of the DCB specimens. It should be mentioned that the aged adhesive layer thickness after abrasion was smaller than 1 mm and the secondary bonding filled the gaps between aged adhesive layer and substrates (see Fig. 1c). The adhesive joints were cured for 25 h at 25 °C according to the manufacturer's technical datasheet. After curing a sharp razor blade was used to make a pre-crack in the middle of the aged adhesive layer manually. Fig. 3 shows the ODCB specimens before (in mould) and after curing.

3.5. Experimental tests

Four kinds of experimental tests were carried out during this research. (1) Gravimetrical, (2) ODCB, (3) DMA, and (4) FTIR tests. In the gravimetrical test at specific exposure time intervals, the specimens were weighed using AB204-S electronic analytical balance (Mettler Toledo, Switzerland) with a precision of 0.1 mg. The water diffusion parameters were determined from the results of the gravimetrical tests. Based on the water content variation at different times and the Fickian law equations (Eq. (5)), the moisture

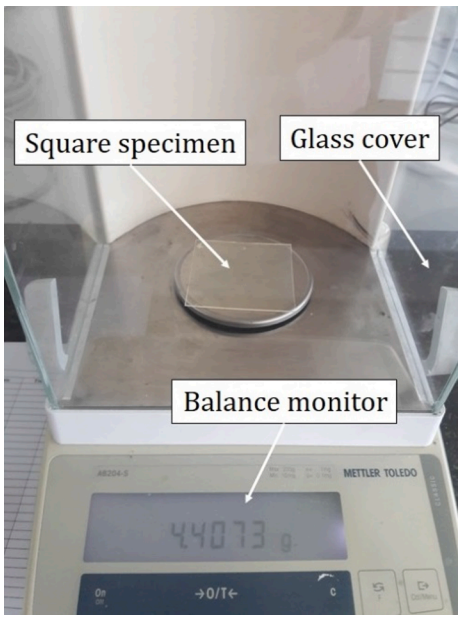

Fig. 4. Weight measurement of square bulk specimen.

diffusion parameters were calculated for all of aging cycles. Five repeats of gravimetrical specimens were tested. The weighing process of square bulk specimen is shown in Fig. 4.

For the ODCB tests, a Zwick tensile test machine, equipped with a 1 kN load cell (with a precision of 0.5 %) was employed. The dissimilar ODCB specimens were tested under a constant displacement rate of 0.5 mm/min. The ODCB tests were carried out at laboratory conditions (temperature of 23 °C and relative humidity of 35 %). Three repeats of each ODCB adhesive joint were tested. Using a digital camera, the crack length and the load-line displacement were recorded during the tests. In order to check the crack propagation path through the aged adhesive layer, a 3D measurement system (Keyence VR-3200 Wide-Area) was used. During this process based on the height of substrate surface and fracture surface the thickness of remained adhesive on fractured substrates can be determined. Different heights on the fracture surface show the cohesive failure inside the aged adhesive layer. The experimental setup of the ODCB tests is shown in Fig. 5.

In order to check the variation of T_g as result of different aging conditions, aged specimens were tested using DMA after the absorption and desorption process in the first, second, and fourth cycles. DMA was conducted using a TA RSA-G2 apparatus. The heating ramp of 3 °C/min was applied from 0 to 100 °C. Three repeats of bulk adhesive specimens were tested in each condition. Based on the DMA results and using the damping ($Tan\delta$) parameter, the T_g values for the unaged and aged adhesives were determined. FTIR analysis was performed on unaged and aged adhesives after the absorption and desorption process in the first, second, and fourth cycles to study the effect of moisture absorption and desorption on the chemical structure of the adhesive. The FTIR spectra have been recorded using Perkin Elmer Spectrum over the region 4100–600 cm^{-1}.

4. Numerical moisture distribution simulation

The moisture diffusion process in the aged primary adhesive layer was simulated using the Finite Element Method (FEM) at different moisture diffusion conditions. In order to simulate moisture content, the moisture diffusion constants obtained from the Fickian law equation (Eq. (5)) were defined as the material property and the final moisture content at the end of each absorption and desorption process was defined as the boundary condition. In the first absorption process simulation, there is no initial moisture in the specimen, but after the first absorption, there is some moisture remaining from the previous diffusion process, which should be considered. In order to apply moisture remaining in the specimen from the previous cycles, the final moisture concentration distribution of each diffusion process was defined as the initial moisture distribution in the next diffusion process. For instance, in numerical simulation of the second absorption, the final moisture distribution of the first desorption was considered as predefined moisture distribution. The numerical simulation was performed using Abaqus software. 8-node quadratic heat transfer or mass diffusion quadrilateral brick (DC2D8) elements were used for the simulation procedure. The most suitable element size was determined based on numerical and experimental moisture uptake comparison which is 2e-5 m. Overall, a total of 12,500 elements were employed. Fig. 6 shows the geometry of the simulated specimen and moisture boundary conditions.

5. Results and discussions

5.1. Moisture absorption–desorption characteristic

The experimental water uptake curves (average of 5 specimens) and theoretical results based on Fick's law equation in the moisture absorption–desorption process of the gravimetrical specimens, for four aging cycles, are shown in Fig. 7. The experimental results were obtained from the gravimetrical tests at different exposure times. Due to the small deviation between the moisture content of specimens, error bars are not visible in Fig. 7. The moisture uptake curves obtained experimentally and Fick's law equations show a good agreement between the results especially after the first cycle (see Fig. 7). It can be concluded that the moisture absorption and desorption follow the Fick's law.

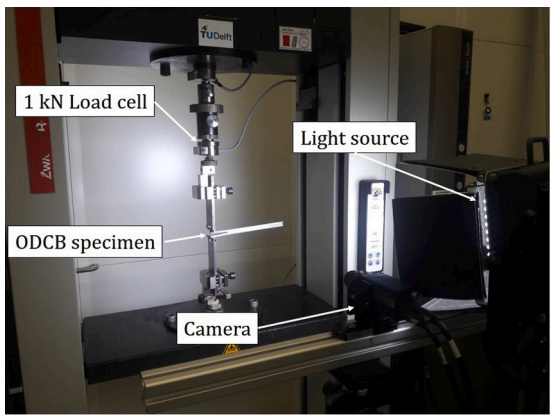

Fig. 5. ODCB test setup.

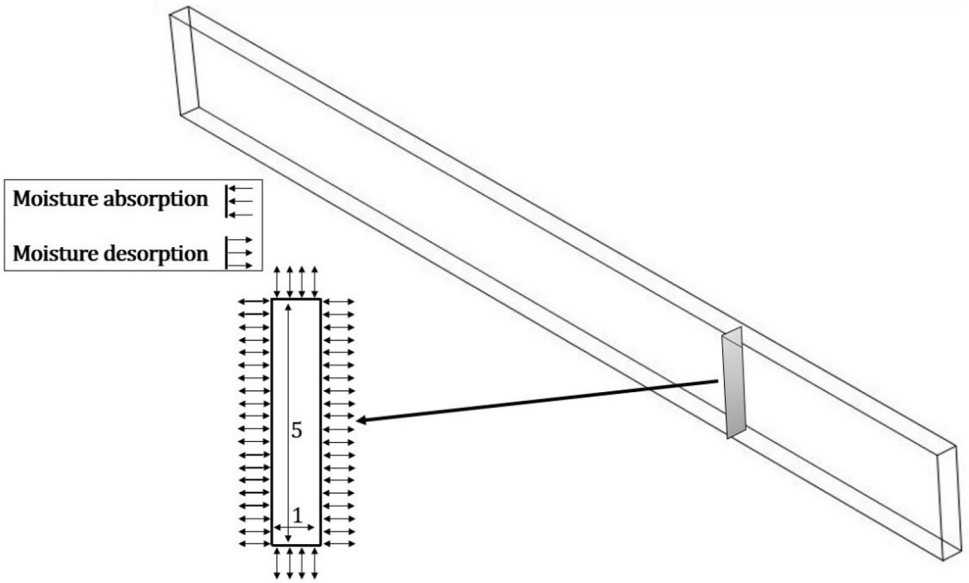

Fig. 6. Schematic of the simulated adhesive specimen and boundary conditions (dimensions in mm).

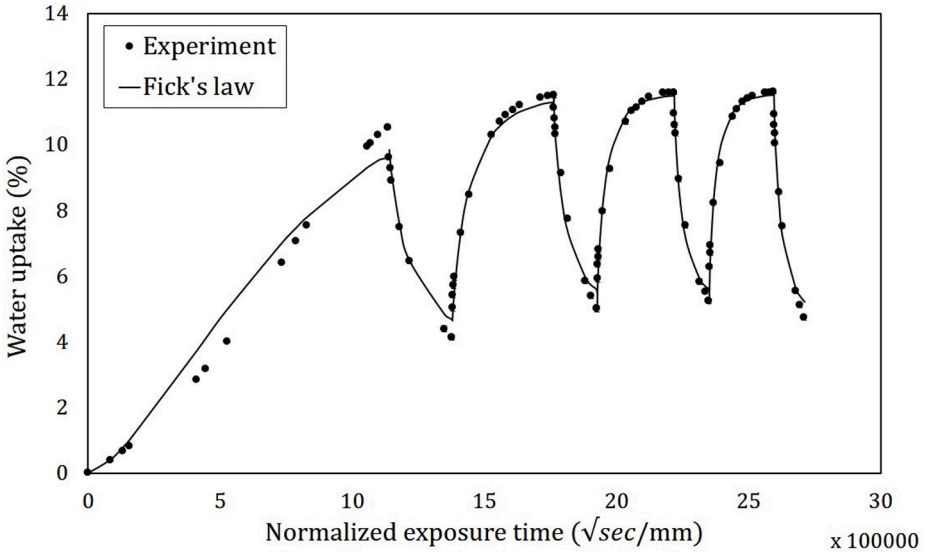

Fig. 7. Experimental and Fick's law curves.

As shown in Fig. 7, the moisture uptake at the end of the absorption and desorption process increases significantly from the first to the second cycle, and after that it remains almost constant. This significant difference between the first and the second cycles is due to incomplete drying of specimen after the first desorption. As a result, after the first cycle, there is still moisture remain in the specimen after the desorption; on the contrary, the first absorption starts when the specimen is completely dried. During the second cycle, due to the initial moisture remaining from the first cycle and larger moisture diffusion rate, the specimen approaches a saturation condition and absorbs water more than the first cycle. The experimental results for different aging cycles are shown in Fig. 8.

As shown in Fig. 8a, the moisture uptake in the first absorption cycle is significantly different from other cycles; on the contrary, the moisture uptake curves in the second, third, and fourth absorption curves are similar. The most important reason for the difference between the first cycle and other cycles is the initial moisture content in the specimen when the different absorption processes started. On the other hand, as shown in Fig. 8b, the comparison of the desorption curves in different cycles show that these curves are close together (especially after the first cycle) and the moisture uptakes in the same exposure time of different cycles are almost the same. It should be mentioned that, in line with the absorption process the difference between the first and other desorption parts is due to the difference in initial moisture uptake at the start of desorption.

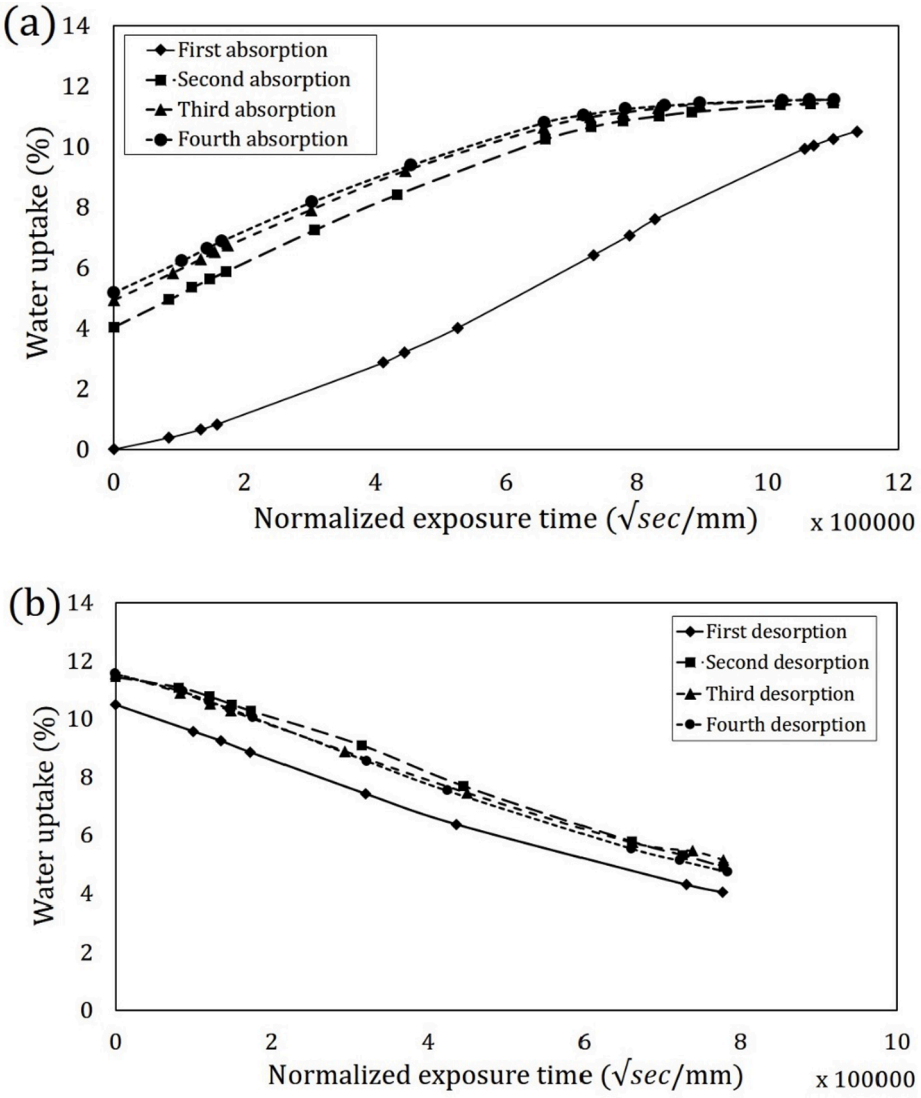

Fig. 8. Experimental moisture absorption (a) and desorption (b) behaviour in different aging cycles (average of 5 specimens results).

Using Eq. (5), the moisture diffusion constant can be calculated based on gravimetrical test results. The moisture diffusion coefficients, and final moisture content at different absorption and desorption cycles are illustrated in Fig. 9.

As can be seen in Fig. 9, the moisture diffusion coefficient in the absorption process increases significantly with the number of aging cycles. The moisture diffusion constant increases more than 3 times between the first and the second absorption. The variation in the moisture diffusion constant can be a result of the changes in the dominant diffusion mechanism and moisture swelling during the absorption. During the absorption process, some mechanisms such as the diffusion of the free water molecules, chemical reaction of water molecules with polymer chains and micro-cracking takes place. Diffusion of free water molecules takes place faster than other mechanisms. As a result, when chemical reaction and micro-cracking are dominant mechanisms during the absorption, the diffusion takes place slowly and moisture diffusion rate is small in comparison with the diffusion of free water molecules. The variation of moisture diffusion constant in different absorption process show that with increasing aging cycles, the chemical reaction and micro-cracking mechanisms decrease and diffusion of free water molecules take place dominantly. Another reason for the significant growing of the rate of moisture diffusion is the swelling. Swelling takes place during the absorption and do not recover completely during the desorption phase. Therefore, the moisture absorption occurs faster during the next absorption process. The experimental results show that after the first cycle, the growth of diffusion constant decreases with each aging cycle. On the other hand, the variation of the diffusion constant in the desorption process is smaller than in the absorption process. The moisture diffusion constant in desorption process increases up to the third aging cycle and decreases after that. The insignificant variation of moisture diffusion constant in desorption processes is due to the diffusion of free water molecules which takes place as a dominant mechanism in all desorption processes [30]. The comparison of moisture diffusion constant in different absorption and desorption processes show that in the first

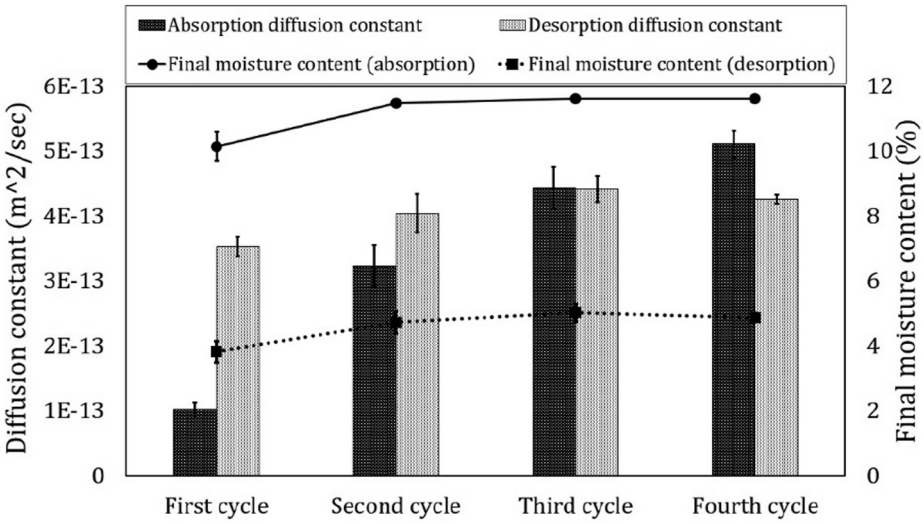

Fig. 9. Diffusion constants and final moisture contents in different absorption and desorption processes.

and second cycles diffusion constants of the absorption process are smaller than the desorption process but in the third and fourth cycles diffusion constant in the absorption process becomes bigger than desorption parts. In other words, after the second cycle, the moisture diffusion in absorption is faster than the desorption process, which is not common in monotonous moisture diffusion [21].

5.2. DMA and FTIR results

DMA and FTIR analysis were performed on unaged and aged specimens after 14 days wetting in the absorption process and 7 days drying in the desorption process at the first, second, and fourth aging cycles. The DMA analysis was conducted in order to measure the T_g of the aged specimens. The DMA results for different aging conditions are shown in Fig. 10a.

Fig. 10a shows variation of damping ($Tan\delta$) in different temperatures. Using the peak point of damping ($Tan\delta$) parameter curves, the T_g of specimens can be determined. The T_g of aged specimens in different aging conditions are illustrated in Fig. 10b.

According to the DMA results, the T_g of the tested adhesive decreases significantly from 49 °C to 32 °C after the first absorption. T_g increases again to 46 °C after the first desorption. This trend remains during the subsequent aging cycles, but the T_g in all aging cycles is lower than for the unaged condition. The reduction in T_g during the absorption process is due to the single hydrogen bound between water molecules and polymer chains. Single hydrogen bounds disrupt the initial Van der Waals force between polymer chains, they increase the polymer chains mobility and consequently decrease the T_g [31]. This kind of the water/adhesive bound has low activation energy and can be removed from the polymer during the desorption process. With decreasing the number of the single hydrogen bounds during the desorption process, T_g increases.

A chemical evaluation using FTIR analysis was made for unaged and aged adhesive at different aging cycles to investigate the effect of repeated moisture absorption and desorption mechanism on the chemical structure of the tested adhesive. Fig. 11 shows the spectrum in the 4000–600 cm^{-1} wavenumber range for unaged and cyclically aged adhesive after the absorption and desorption process for the first, second, and fourth aging cycles. The spectrums of unaged and aged specimens show several same peaks. The peaks at 1509 and 825 cm^{-1} can be assigned to p-phenylene groups. The characterization of the spectrum diglycidyl ether of bisphenol (DGEBA) molecules can be done by some absorption peaks such as: the aliphatic carbon–oxygen (1035 cm^{-1}) and the aromatic carbon oxygen stretching (strong band at 1244 cm^{-1}). There is a peak at 2922 cm^{-1}, due to the stretching vibration of the $-CH_2-$ groups. The peaks at 3296 cm^{-1} can be a result of the chemical bond between polymer chains and water molecules. The comparison of spectrums for different aging conditions shows a small difference in chemical structure for the unaged and aged specimens (see Fig. 11) in peak at 3296 cm^{-1}. As can be seen in Fig. 11 (magnified part) with the aging cycles the peaks of the absorption and desorption curves increases for the 3296 cm^{-1} wave number. It means that the amount of chemical bound between the polymer and water increases with aging cycles. In absorption process there is a significant difference between the first and the second absorption while the second and fourth absorption curves are close together. The obtained curves for different absorption and desorption processes show that after the desorption process the chemical bound between the water and polymer chains decreases. This reduction is related to the breaking of single hydrogen bounds during the desorption stage. The remained peaks after the desorption process show that there are some multiple hydrogen bounds between water molecules and polymer chains with high activation energy which cannot be removed during the drying process. The FTIR curves show a good agreement with the moisture uptake curves in different cycles as shown in Fig. 7. The peak in the unaged specimen curve shows chemical water bound, which can be due to the initial moisture bonding absorbed during the fabrication process and moisture absorption during the FTIR test.

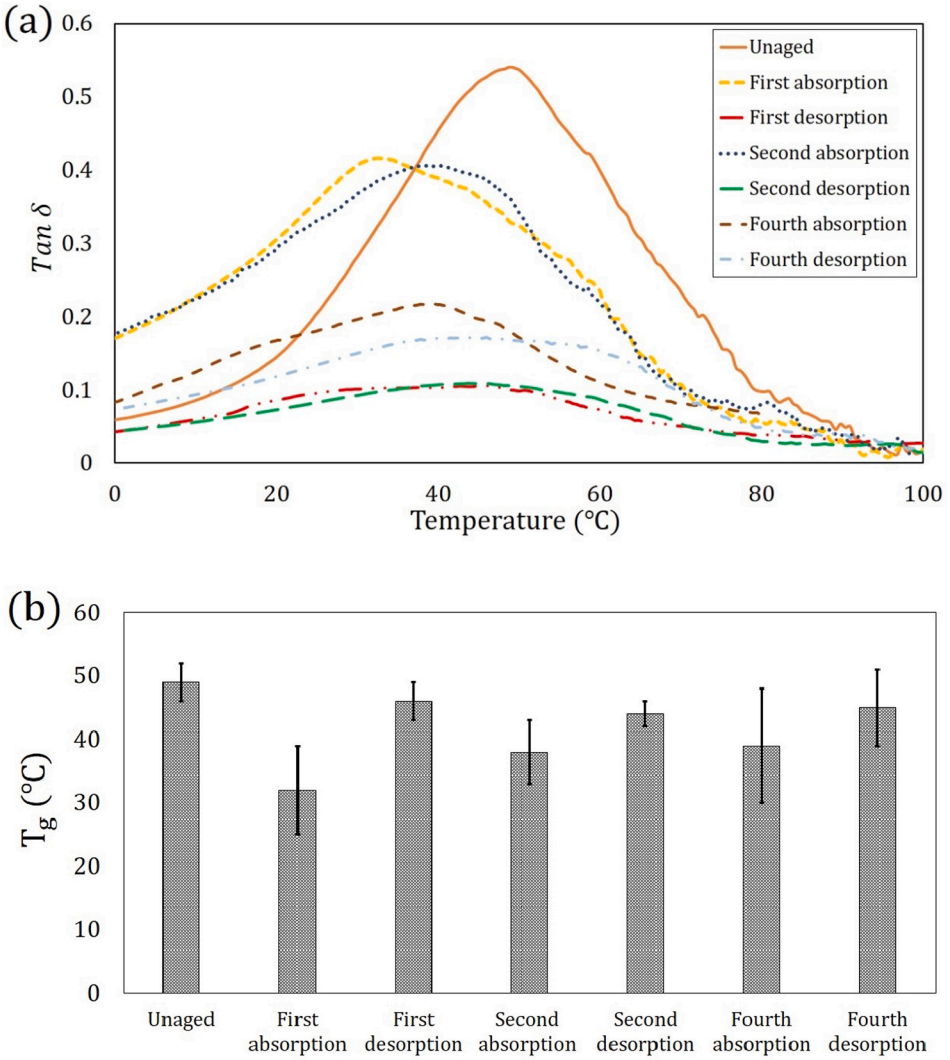

Fig. 10. Damping changes at different temperature for different aging conditions (a) and T_g of aged adhesive in different aging cycles (b).

5.3. Mode I fracture energy

Mode I fracture tests of ODCB adhesive joints for both the aged and unaged adhesive joints were performed in order to investigate the effects of cyclic aging on mode I fracture energy of dissimilar GFRP-Al ODCB joints. The load–displacement curve of unaged specimen is illustrated in Fig. 12a. In order to analyse the crack propagation path through the aged adhesive layer, a 3D measurement system (Keyence VR-3200 Wide-Area) was used. During this process based on the roughness of the fracture surface and the thickness of the substrate the thickness of the reamaining adhesive on the fractured surface was determined. Accordingly, the cohesive failure through the aged adhesive layer was confirmed as shown in Fig. 12b.

Due to the dissimilarity in substrates of adhesive joints, using the SBT equation for mode I fracture energy calculation is challenging. In the SBT relation (Eq. (8)) the thickness, tensile, and shear elastic modulus of one of the substrates were considered. Consequently, for adhesive joints with the same substrates, both substrates can be considered in the SBT equation, but in dissimilar adhesive joints the thickness and tensile and shear elastic modulus of the substrates are different. In dissimilar adhesive joints designed based on the equality of the flexural stiffness of substrates the SBT equation is not sensitive to the chosen substrate and both substrates can be considered in the SBT equation. In this study, in order to reach the pure mode I loading condition, ODCB adhesive joints were designed based on the longitudinal strain criterion (using Eq. (9)). In dissimilar DCB adhesive joints designed based on the longitudinal strain criterion, the flexural stiffness of substrates is different and accordingly, the calculated mode I fracture energy based on different substrates will lead to different results. It means that SBT results are sensitive to the chosen substrate in this condition. In order to check the accuracy of SBT for mode I fracture energy calculation, the mode I fracture energy of unaged dissimilar adhesive joints were calculated using different approaches such as FEM and Penado-Kanninen (PK) model. PK model which proposed for energy release rate

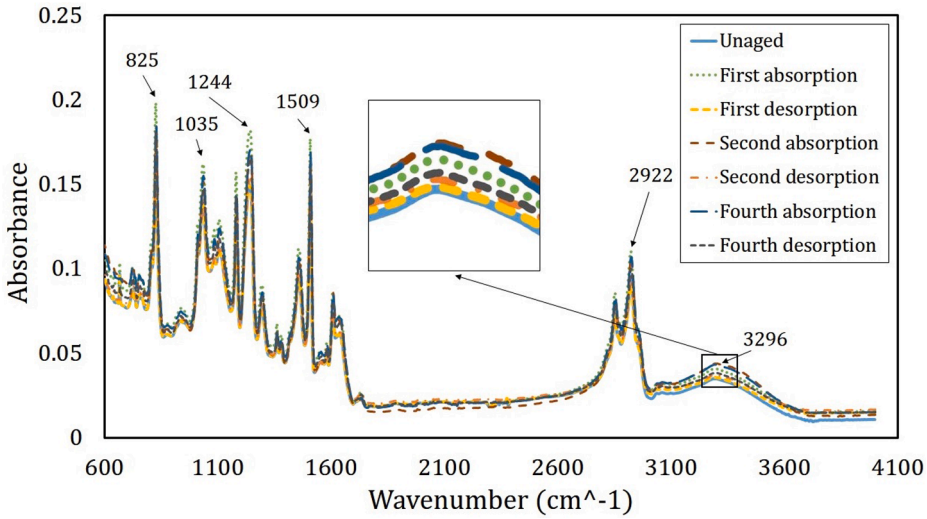

Fig. 11. FTIR spectrum, in the 4000–600 cm^{-1} wavenumber range for unaged and aged specimens in different aging conditions.

calculation of DCB joints by previous investigators [32,33] was used in this study. This model has been already developed and verified for fracture energy calculation of dissimilar DCBs by other authors [8]. The details of the fracture energy calculation using PK model can be found in [8]. In this process, the flexural and out of plane shear modulus of the GFRP laminate were considered as 21,014 and 4125 MPa, respectively [12]. In addition, the details of the numerical simulation process using the FEM can be found in [34]. The comparison of obtained mode I fracture energy from different methods shows that the SBT with aluminum as substrates agrees very well with the PK model. Accordingly, SBT with Al substrates is accurate enough to get the fracture energy of the dissimilar DCBs tested. The comparison of PK model and SBT results shows that the maximum difference between SBT (with aluminum substrate) and PK model is about 7 %. Therefore, for the calculation of the mode I fracture energy of cyclically aged dissimilar DCBs, the SBT (considering aluminum for both substrates) was used.

The calculation of mode I fracture energy was conducted for the first, second, and fourth cycles based on load–displacement curves. The variation of mode I fracture energy for different exposure times in the first, second and fourth cycles (see Fig. 2b) are shown in Fig. 13.

As can be concluded from Fig. 13, during the fracture test of different specimens, the crack propagates in two or three steps and fracture energy can be measured in two or three different crack lengths (see Fig. 12a). R-curves show that the fracture energy obtained from the initial crack length (pre-crack created by razor blade manually) is slightly larger than other crack lengths. This difference is mainly due to the crack tip condition for the initial pre-crack, which is not usually a perfect sharp crack. The reported fracture energy in this study is the average fracture energy of three tested ODCB specimens. Fig. 14 shows that fracture energy decreases by aging time and with the aging cycles.

Fracture tests were carried out also during the desorption process. This process was repeated for the first, second, and fourth desorption. The mode I fracture energy as a function of crack length during the drying process is shown in Fig. 15.

As can be seen in Fig. 15, during the desorption process mode I fracture energy increases by drying time. The fracture energy curves of desorption cycles show that during the desorption process before 2 days, fracture energy increase significantly and after 2 days drying this parameter changes slowly. Fig. 16 displays the mode I fracture energy at different drying times of different desorption cycles.

As shown in Fig. 16 by increasing the drying time the sensitivity of fracture energy to aging cycles decreases. In order to compare mode I fracture energy in the same moisture content in different absorption and desorption process, numerical simulation of moisture diffusion in different aging cycles are needed.

5.4. Moisture distribution simulation

The moisture concentration distribution of the adhesive layer cross-section (see Fig. 6) was simulated numerically based on the moisture diffusion parameters such as the diffusion constant and the moisture contents calculated from the gravimetrical test at the end of the absorption and desorption processes. In order to simulate moisture concentration, the final moisture content obtained from gravimetrical tests was defined as the boundary condition. For instance, in the second absorption process, the moisture concentration in specimen boundaries was considered by 11.47 %, which is moisture uptake after the second absorption. The moisture content of different elements in different exposure times during the second adsorption and desorption are illustrated in Figs. 17 and 18, respectively.

As shown in Fig. 17a, the moisture content in the adhesive layer before starting the absorption is more than 3.83 %, which is due to the moisture remaining from the first cycle. When the absorption process starts, the moisture diffuses into the specimen. The obtained

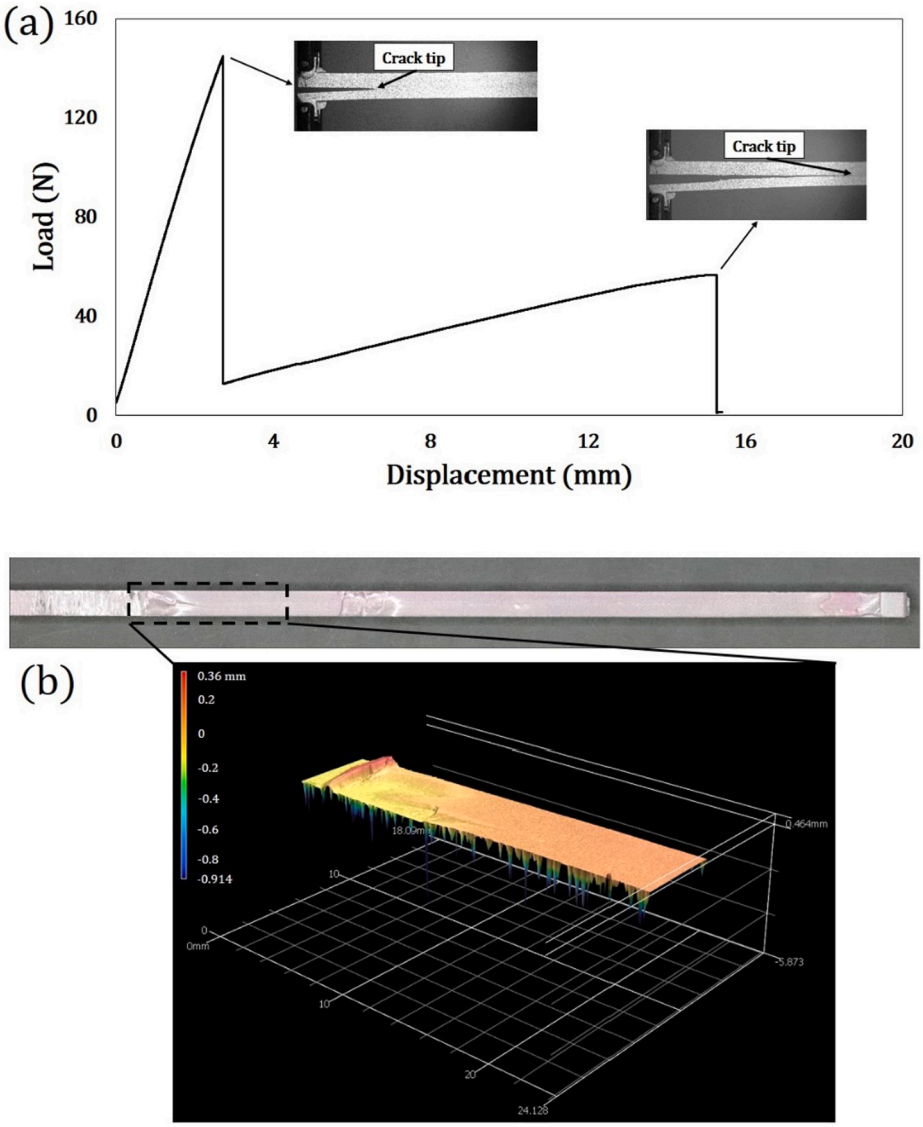

Fig. 12. Load-displacement curve (a) and 3D scan of surface fracture near the crack tip (b).

results show that after 8 h the moisture concentration of a thin layer of the specimen surface reaches 11.51 % and with increasing exposure time this layer becomes thicker and the moisture concentration of the specimen increases. After 14 days, the moisture concentration of the specimen in different elements changes between 11.51 %and 11.21 %. It means that moisture content in most elements is close to maximum moisture uptake in second absorption (11.47 %).

In the drying process, the moisture content decreases with drying time (see Fig. 18). After 8 h drying, a thin layer around the specimen reaches to moisture concentration of 4.72 %. With increasing drying time, this layer becomes thicker and the moisture content of the specimen decreases. The moisture concentration in the specimen after 7 days desorption in different elements is between 4.72 % and 5.57 %. In order to obtain the mode I fracture energy of aged specimens as a function of moisture diffusion conditions, the average moisture content of specimens was calculated at different exposure times. For this purpose, the moisture concentration parameter of specimen elements was averaged at different times and aging cycles. Fig. 19 represents the averaged moisture content at different exposure times numerically obtained using FEM.

As expected, except for the first cycle the moisture content curves for different cycles are very close to each other. In order to verify the moisture distribution simulation obtained from FEM, the moisture uptakes of the second cycle, obtained from FEM were compared with the results of gravimetrical tests and Fick's law. Fig. 20 represents the moisture uptake obtained from different approaches in second absorption and desorption.

As shown in Fig. 20, the moisture content of the specimen in the second cycle obtained using different methods are very close together. It means that FEM simulation based on Fick's law equation is suitable for modelling the moisture concentration distribution

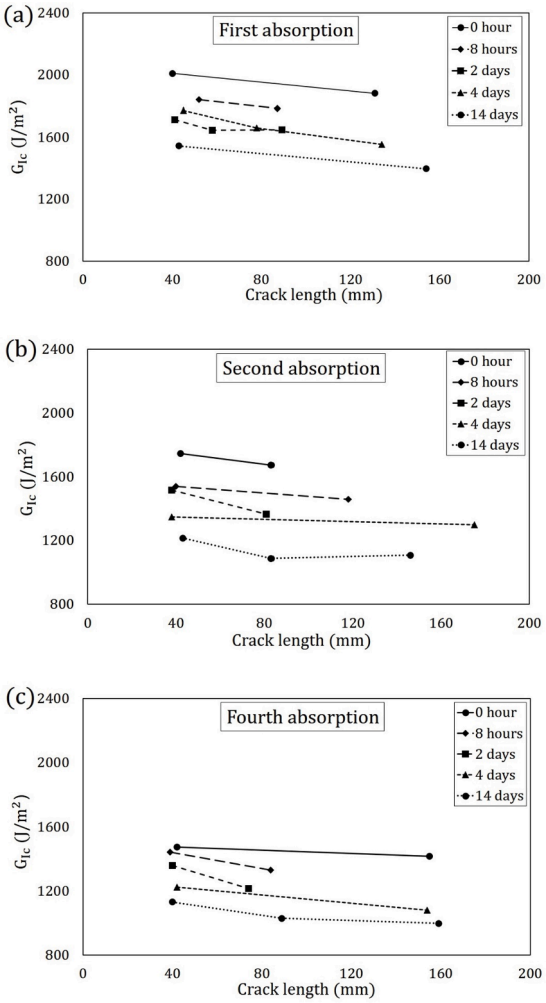

Fig. 13. Mode I fracture energy in different exposure times during the absorption of first (a), second (b) and fourth (c) cycles.

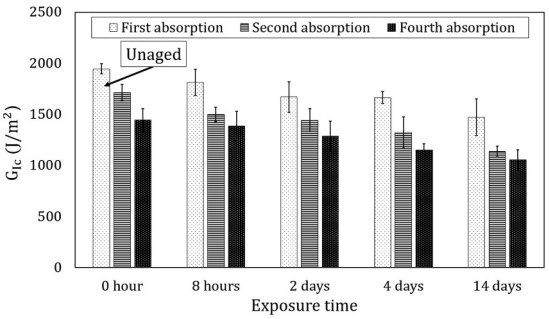

Fig. 14. Variation of mode I fracture energy in different exposure times of absorption process.

in the tested specimens. The comparison of moisture content of different methods shows that, in the absorption process, moisture content simulated by FEM is bigger than other methods, while in the desorption process, FEM moisture contents are smaller than the results of experimental and Fick's law. The difference between the results of FEM and other methods is due to the difference between the dimension of the adhesive layer and gravimetrical specimens. Two-dimensional moisture diffusion takes place in the adhesive layer (see Figs. 17 and 18), but in gravimetrical specimens, one-dimensional moisture diffusion occurs. Based on moisture concentration simulated numerically for different aging conditions, and using the experimental fracture tests results, the variation of fracture energy can be represented as a function of moisture content and aging cycles as shown in Fig. 21.

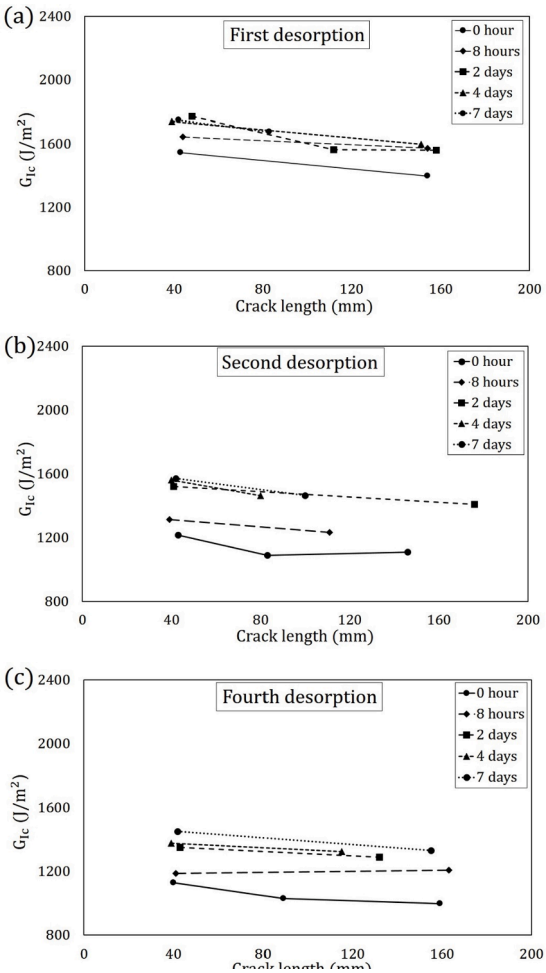

Fig. 15. Mode I fracture energy in different drying times during the first (a), second (b) and fourth (c) desorption.

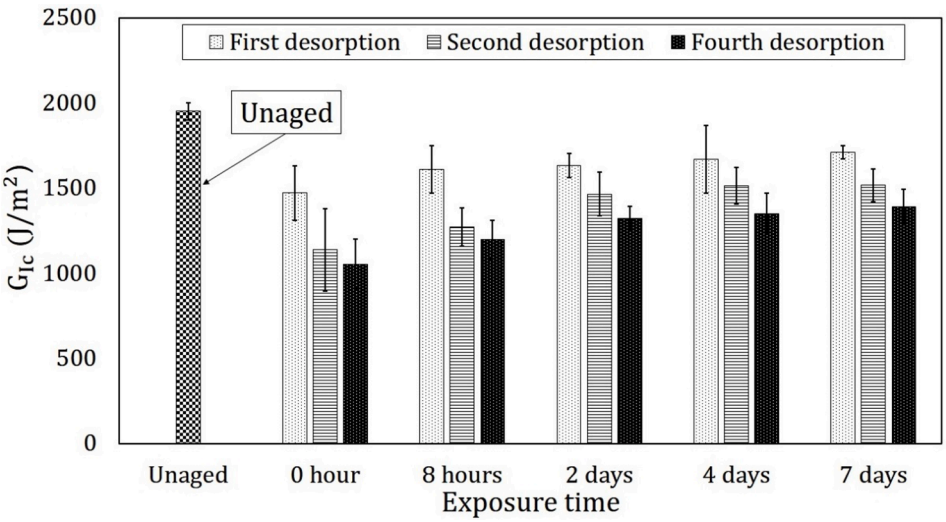

Fig. 16. Variation of mode I fracture energy in different exposure times of desorption process.

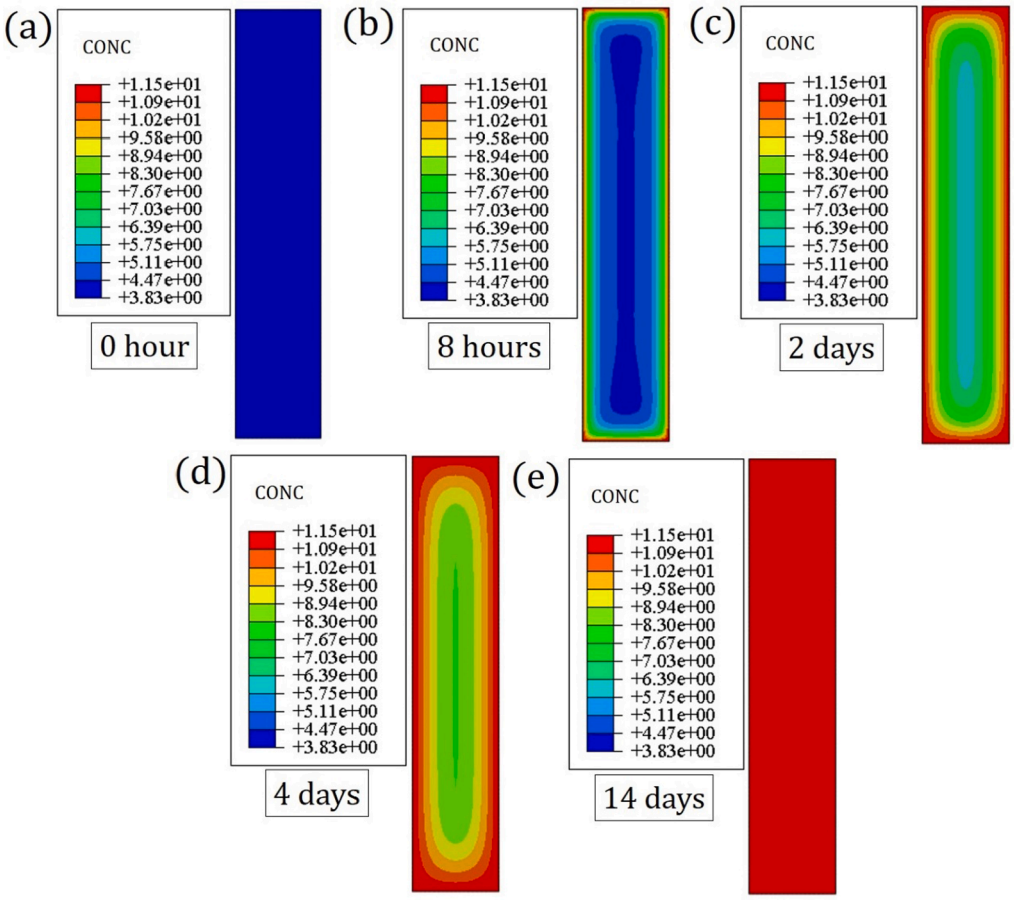

Fig. 17. Moisture concentration distribution on adhesive layer cross-section (in percentage) for unaged (a) and after 8 h (b), 2 days (c), 4 days (d), and 14 days (e) aging for the second absorption cycle.

As illustrated in Fig. 21, during the absorption process with increasing the exposure time and moisture content the fracture energy decreases and in the drying process with increasing of drying time the fracture energy increases. The results presented in Fig. 21 show that the mode I fracture energy during the absorption and desorption is a function of aging cycles and moisture content. In other words, the mode I fracture energy is sensitive to aging cycles and for analysis of adhesive joints exposed to cyclic aging conditions, the obtained results from monotonous moisture tests are not reliable and the cyclic aging test is needed. It means that specimens with more moisture content are less sensitive to aging cycles than dried specimens. In addition, the results showed that by increasing the number of ageing cycles the sensitivity of mode I fracture energy to aging cycles decreases.

The variation of the fracture energy in each cycle including the absorption and desorption processes is illustrated in Fig. 22.

As shown in Fig. 22a, in the first aging cycle, the fracture energies of the adhesive after the adsorption and desorption processes in the same moisture content are close together. With the aging cycles, the difference between the absorption and desorption fracture energies increases. It was also found that at similar moisture content, the fracture energy of the desorption process is smaller than that in the absorption process at each aging cycle (see Fig. 22b and c).

6. Conclusions

In this paper the effect of cyclic aging on mode I fracture energy of dissimilar DCB adhesive joints was investigated. For this purpose, the moisture adsorption and desorption behaviour of adhesive specimens in different aging cycles were studied. Then, using the load–displacement curves obtained from the fracture tests of DCB including an aged adhesive layer, mode I fracture energy at different moisture contents was calculated. Finally, based on FEM simulation, the variation of mode I fracture energy at different moisture diffusion conditions was investigated. According to the obtained results, the following conclusions can be drawn:

- In cyclic aging, the diffusion constant and the final moisture contents in absorption and desorption processes increase by aging cycles. The moisture diffusion constant in the absorption process is more sensitive to aging cycles than the desorption process constant.

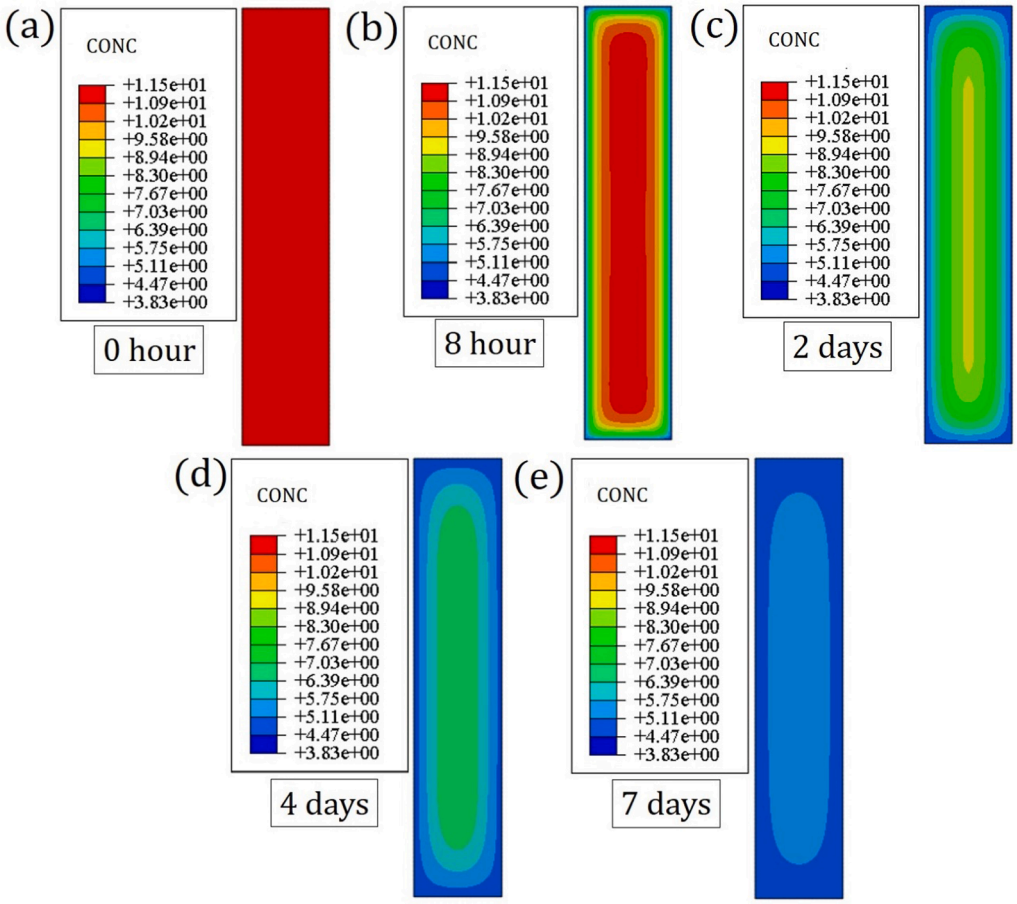

Fig. 18. Distribution of moisture concentration of adhesive layer cross-section (in percentage) after 0 (a) and 8 (b) hours, and after 2 (c), 4 (d), and 7 (e) days drying for the second desorption cycle.

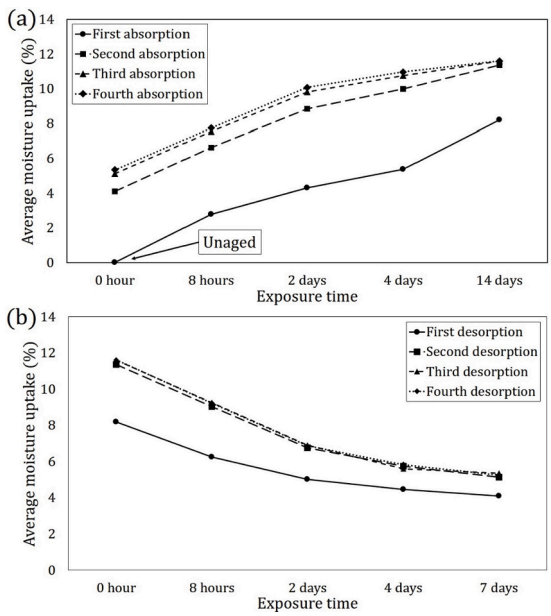

Fig. 19. Simulated moisture content for different exposure times in the absorption (a) and desorption (b) processes.

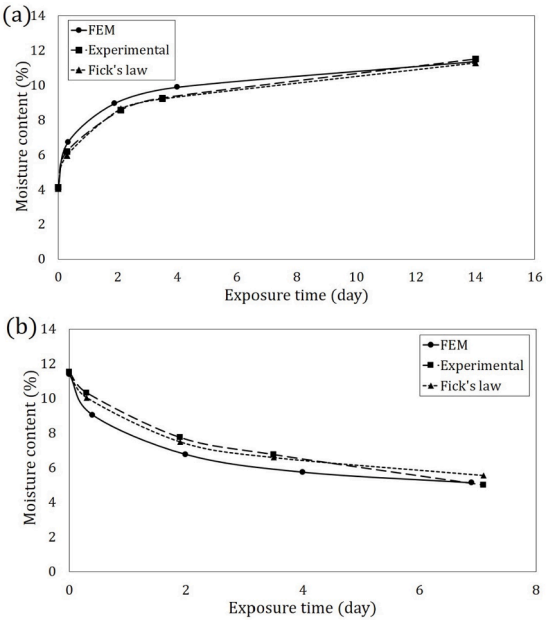

Fig. 20. Moisture contents obtained from different approaches in the second absorption (a) and desorption (b) processes.

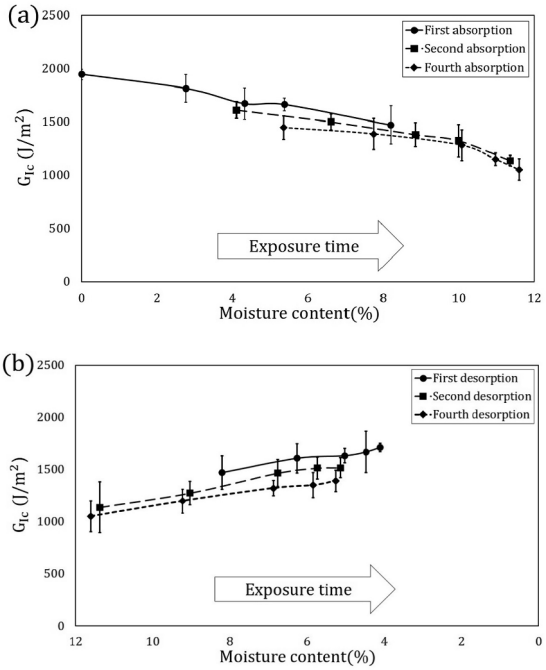

Fig. 21. Mode I fracture energy variation in different moisture uptakes in absorption (a) and desorption (b) processes.

- The variation of moisture diffusion parameters such as moisture diffusion constant and final moisture uptake decrease with aging cycles specifically after the first cycle.
- In the first and second cycles the diffusion constant of the absorption process is smaller than the desorption process. Due to a significant increase of the diffusion constant in the absorption process in the third and fourth cycles the diffusion constant of the absorption process becomes bigger than that in desorption process.
- For the Araldite 2011 adhesive, mode I fracture energy decreases with moisture content, and increases with drying.
- In each cycle the fracture energy reduction during the moisture absorption is more than fracture energy recovery during the moisture desorption.

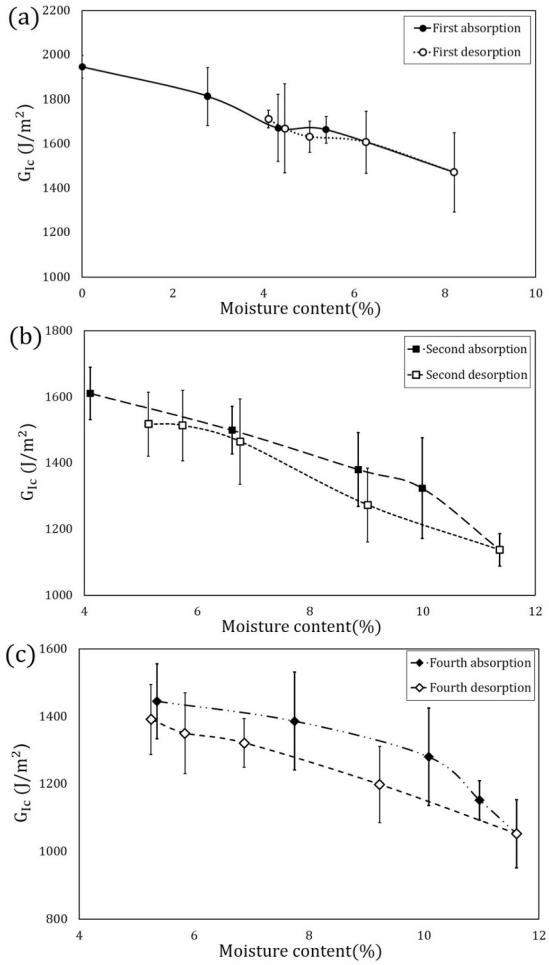

Fig. 22. Mode I fracture energy variation during the first (a), second (b) and fourth (c) cycles.

- During the moisture absorption the glass transition temperature decreases and with drying specimens this parameter increases. In different cycles, the fluctuation of glass transition temperature decreases with the increase of aging cycles.
- The combination of experimental and numerical results shows that by increasing the number of aging cycles, the rate of reduction in mode I fracture energy between the aging cycles decreases.

CRediT authorship contribution statement

M. Moazzami: Writing – review & editing, Writing – original draft, Investigation, Data curation. **M.R. Ayatollahi:** Supervision, Project administration. **A. Akhavan-Safar:** Writing – review & editing, Supervision, Methodology, Conceptualization. **S. Teixeira De Freitas:** Writing – review & editing, Methodology, Supervision. **J.A. Poulis:** Writing – review & editing, Validation, Methodology. **L.F. M. da Silva:** Writing – review & editing, Supervision.

Declaration of Competing Interest

The authors declare that they have no known competing financial interests or personal relationships that could have appeared to influence the work reported in this paper.

Data availability

The data that has been used is confidential.

References

[1] Banea MD, da Silva LF, Campilho RD, Sato C. Smart adhesive joints: An overview of recent developments. J Adhes 2014;90(1):16–40.
[2] Banea MD, da Silva LF. Adhesively bonded joints in composite materials: an overview. Proc Instit Mech Eng, Part L: J Mater: Des Appl 2009;223(1):1–18.
[3] Mouritz AP, Gellert E, Burchill P, Challis K. Review of advanced composite structures for naval ships and submarines. Compos Struct 2001;53(1):21–42.
[4] Eslami S, Taheri-Behrooz F, Taheri F. Effects of aging temperature on moisture absorption of perforated GFRP. Adv Mater Sci Eng 2012;2012.
[5] Wang W, De Freitas ST, Poulis JA, Zarouchas D. A review of experimental and theoretical fracture characterization of bi-material bonded joints. Compos B Eng 2020:108537.
[6] Budhe S, Banea M, De Barros S, Da Silva L. An updated review of adhesively bonded joints in composite materials. Int J Adhes Adhes 2017;72:30–42.
[7] Fernandes RL, Budzik MK, Benedictus R, de Freitas ST. Multi-material adhesive joints with thick bond-lines: Crack onset and crack deflection. Compos Struct 2021;266:113687.
[8] Fernandes RL, de Freitas ST, Budzik MK, Poulis JA, Benedictus R. Role of adherend material on the fracture of bi-material composite bonded joints. Compos Struct 2020;252:112643.
[9] A. Standard, ASTM Standard D3433-99, 2020, Standard Test Method for Fracture Strength in Cleavage of Adhesives in Bonded Metal Joints, ASTM International, West Conshohocken, PA, ed, 2020.
[10] Fernandes RL, de Freitas ST, Budzik MK, Poulis JA, Benedictus R. From thin to extra-thick adhesive layer thicknesses: Fracture of bonded joints under mode I loading conditions. Eng Fract Mech 2019;218:106607.
[11] Jespersen KM, Ota H, Harada K, Hosoi A, Kawada H. Experimental measurement of mode-I fracture toughness of dissimilar material joints with thermal residual stresses. Eng Fract Mech 2020;238:107249.
[12] Wang W, Fernandes RL, De Freitas ST, Zarouchas D, Benedictus R. How pure mode I can be obtained in bi-material bonded DCB joints: a longitudinal strain-based criterion. Compos B Eng 2018;153:137–48.
[13] Khoshravan M, Mehrabadi FA. Fracture analysis in adhesive composite material/aluminum joints under mode-I loading; experimental and numerical approaches. Int J Adhes Adhes 2012;39:8–14.
[14] Chalmers D. The potential for the use of composite materials in marine structures. Mar Struct 1994;7(2–5):441–56.
[15] Hua Y, Crocombe A, Wahab M, Ashcroft I. Modelling environmental degradation in EA9321-bonded joints using a progressive damage failure model. J Adhes 2006;82(2):135–60.
[16] Khoramishad H, Alizadeh O. Effects of silicon carbide nanoparticles and multi-walled carbon nanotubes on water uptake and resultant mechanical properties degradation of polymer nanocomposites immersed in hot water. Polym Compos 2018;39(S2):E883–90.
[17] Sugiman S, Crocombe A, Aschroft I. Experimental and numerical investigation of the static response of environmentally aged adhesively bonded joints. Int J Adhes Adhes 2013;40:224–37.
[18] Fernandes P, Viana G, Carbas R, Costa M, Da Silva L, Banea M. The influence of water on the fracture envelope of an adhesive joint. Theor Appl Fract Mech 2017;89:1–15.
[19] Rodrigues TA, Chaves FJ, Silva LFd, Costa M, Barbosa AQ. Determination of the fracture envelope of an adhesive joint as a function of moisture: Bestimmung der Bruchumgebung für das Versagen einer Klebeverbindung als Funktion der Feuchtigkeit. Materialwissenschaft und Werkstofftechnik 2017; 48(11): 1181–1190.
[20] Zheng G, et al. On failure mechanisms in CFRP/Al adhesive joints after hygrothermal aging degradation following by mechanical tests. Thin-Walled Struct 2021;158:107184.
[21] Mubashar A, Ashcroft IA, Critchlow GW, Crocombe A. Moisture absorption–desorption effects in adhesive joints. Int J Adhes Adhes 2009;29(8):751–60.
[22] Da Costa J, Akhavan-Safar A, Marques E, Carbas R, Da Silva L. Cyclic ageing of adhesive materials. J Adhes 2021:1–17.
[23] Khoramishad H, Bayati H, Kordzangeneh D. The deleterious effect of cyclic hygrothermal aging on nanocomposite adhesives. J Adhes 2020:1–19.
[24] Crank J. The Mathematics of Diffusion. London: Oxford Univ. Press; 1975.
[25] Datla N, Ameli A, Azari S, Papini M, Spelt J. Effects of hygrothermal aging on the fatigue behavior of two toughened epoxy adhesives. Eng Fract Mech 2012;79:61–77.
[26] Costa M, Viana G, da Silva L, Campilho R. Effect of humidity on the mechanical properties of adhesively bonded aluminium joints. Proc Instit Mech Eng, Part L: J Mater: Des Appl 2018;232(9):733–42.
[27] Kanninen M, Popelar C, Saunders H. Advanced fracture mechanics. Oxford: Oxford University Press; 1988.
[28] Chaves FJ, Da Silva L, De Moura M, Dillard D, Esteves V. Fracture mechanics tests in adhesively bonded joints: a literature review. J Adhes 2014;90(12):955–92.
[29] Costa M, et al. Effect of the size reduction on the bulk tensile and double cantilever beam specimens used in cohesive zone models. Proc Instit Mech Eng, Part L: J Mater: Des Appl 2016;230(5):968–82.
[30] Mubashar A, Ashcroft IA, Critchlow GW, Crocombe A. Modelling cyclic moisture uptake in an epoxy adhesive. J Adhes 2009;85(10):711–35.
[31] Zhou J, Lucas JP. Hygrothermal effects of epoxy resin. Part II: variations of glass transition temperature. Polymer 1999;40(20):5513–22.
[32] Kanninen M. An augmented double cantilever beam model for studying crack propagation and arrest. Int J Fract 1973;9(1):83–92.
[33] Penado F. A closed form solution for the energy release rate of the double cantilever beam specimen with an adhesive layer. J Compos Mater 1993;27(4):383–407.
[34] Moazzami M, Ayatollahi M, de Freitas ST, da Silva L. Towards pure mode I loading in dissimilar adhesively bonded double cantilever beams. Int J Adhes Adhes 2021;107:102826.